Journal of Applied Physics METHOD pubs.aip.org/aip/jap

Defect investigation of undoped wide bandgap materials: Comparison between charge transient spectroscopy (QTS) and inverse Laplace QTS

Cite as: J. Appl. Phys. **137**, 155701 (2025); doi: 10.1063/5.0257511
Submitted: 10 January 2025 · Accepted: 26 March 2025 ·
Published Online: 15 April 2025

Rina Yamazaki,[1,a)] Jan Isberg,[1] Nattakarn Suntornwipat,[1] Dmitrii Moldarev,[2] Björn Magnusson,[3] Aisuluu Aitkulova,[1] and Saman Majdi[1]

AFFILIATIONS

[1]Division of Electricity, Department of Electrical Engineering, Uppsala University, Box 65, 751 03 Uppsala, Sweden
[2]Division of Materials Physics, Department of Physics and Astronomy, Uppsala University, Box 516, 751 20 Uppsala, Sweden
[3]STMicroelectronics Silicon Carbide AB, Ramshällsvägen 15, 602 38 Norrköping, Sweden

[a)]**Author to whom correspondence should be addressed:** rina.yamazaki@angstrom.uu.se

ABSTRACT

Understanding the electrically active defects and impurities in semiconductors, especially in intrinsic or unintentionally doped wide bandgap materials, still remains a challenge. Here, time-of-flight (ToF) measurement using a solid state light source (355 and 213 nm) was performed on intrinsic silicon carbide and single-crystalline diamond. The charge transient spectroscopy (QTS) and the inverse Laplace (IL) QTS methods were applied to analyze the ToF results. Using these methods, we were able to trace the existing impurities in both materials. However, ILQTS proved to be more sensitive, with higher resolution for detection of existing multiple defects. The results suggest that this system can successfully be employed to investigate electrically active impurities at different energy states in highly resistive and undoped materials.

I. INTRODUCTION

Investigation of defects in wide bandgap materials is one of the exciting topics for understanding the characteristics of materials for power electronics.[1] Many studies have been done optically and electrically to address and reveal the nature of some of these defects. However, electrical detection of the impurities in such materials is not straightforward due to the lack of free charges.

Transient spectroscopy is an experimental technique to electrically investigate defects in semiconductors. Deep-level transient spectroscopy (DLTS)[2,3] is one of the most common techniques. DLTS measures the capacitance transient in the depletion region at different temperatures, which gives, in the end, an Arrhenius plot to find the defect energy level. The technique has its limitation since a p-n junction or Schottky structure is necessary for the measurement. Wide bandgap (high resistive) semiconductors are sometimes unsuitable for DLTS because it is difficult to calculate capacitance accurately from small currents. The same is valid for undoped materials.[4] To improve sensitivity, scanning ion deep-level transient spectroscopy (SIDLTS)[5] was invented. Even though sensitivity has increased, it still has the structure limitations of the conventional DLTS techniques.

Charge transient spectroscopy (QTS)[6,7] is another technique for transient spectroscopy and a good alternative to DLTS. It can be used even when materials are highly resistive or undoped. QTS requires a much simpler contact configuration, ohmic contacts, on the top and back surfaces of the target semiconductor. Here, free charge is generated by an external source. The back contact measures the current that is induced by the charges. The data analysis is similar to DLTS. Depending on the source of radiation, the method is referred to as alpha particle induced charge transient spectroscopy (APQTS)[8] and heavy ion induced charge transient spectroscopy (HIQTS).[9] Furthermore, to improve resolution, an analyzing method using the inverse Laplace transformation was introduced. It finds activation energies directly by fitting the

current data and applying inverse Laplace transformation to the fitting result. Many studies have been performed to apply this method to DLTS,[10–13] but there are fewer studies that have been made for QTS on undoped wide bandgap materials.

This paper shows the comparison of two methods, QTS and ILQTS, as a proof of concept for investigation of intrinsic defects. Time-of-flight (ToF) measurement was performed as a laser QTS technique. Two unintentionally doped wide bandgap materials, silicon carbide (4H-SiC) and single crystalline diamond (SCD), were selected. These wide bandgap materials (3.26 eV and 5.47 eV, 4H-SiC and diamond, respectively) have interesting electrical properties for many applications, e.g., power electronics. Thus, understanding the defects and impurities in these materials is essential.[14,15] Both substrates used here are highly resistive (intrinsic), without containing any intentional impurities. Hence, in this case, a defect study and the impact on the electronic properties are not possible with conventional systems, such as DLTS measurements. This study shows the methodology of using ToF technique as QTS for defect investigation and the sensitivity of the two analyzing methods.

II. MATERIALS AND EXPERIMENTAL SETUP

A. Samples

A silicon carbide (SiC) wafer prepared by STMicroelectronics Silicon Carbide AB was used in this study. The SiC wafer is of the 4H polytype with 2 in. diameter, on-axis orientation, and a thickness of 350 μm. The front surface (Si-face) is epi-ready CMP polished and the backside (C-face) is with an optical polish. The samples have an average resistivity of 10^{10}–10^{12} Ω cm. The substrates are grown with the high-temperature chemical vapor deposition (HTCVD) method and no intentional doping was applied. Using a dicing saw with a diamond blade, the wafer was cut into 5×5 mm squares and a sample from the middle part of the wafer was selected for the measurement. In addition, a free-standing commercially available CVD single crystalline diamond substrate with sub-ppm level of impurities was selected for this study. The diamond substrate used is 4×4 mm in size, with a thickness of 110 μm, and grown in the (100) direction.

Prior to device fabrication, both substrates were cleaned in strongly oxidizing solutions to remove any residual surface conductivity. The samples were boiled in a graphite etch ($HNO_3 : H_2SO_4 : HClO_4, 1:1:1$) for 40 min at $\sim 180^{\circ}C$ and oxygen-terminated in an oxygen plasma for 60 s. A semitransparent Ti/Al (15/200 nm) mesh top contact was deposited by a Von Ardenne Magnetron Sputter on both samples to allow optical access and at the same time obtain a homogeneous electric field in the sample.[16] This was followed by depositing a solid Ti/Al (15/200 nm) ohmic contact on the entire backside.

B. ToF setup

The ToF measurement, which uses the QTS technique, is primarily employed to assess charge transient properties[17–21] in intrinsic materials such as diamond (an illustration is shown in Fig. 1). The free charge carriers in our ToF system are generated by using a short light pulse of 800 ps (FWHM) from tripled and quintupled

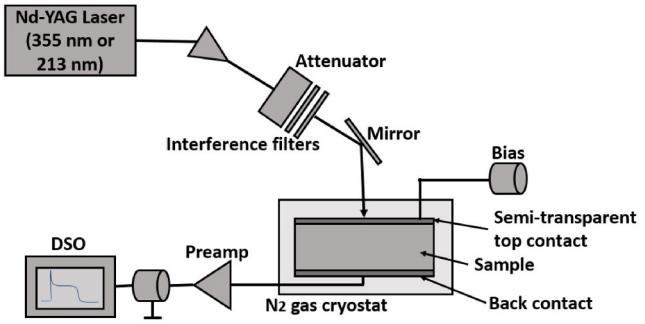

FIG. 1. Illustration of the ToF system with a 355 or 213 nm laser. Using the laser, the charges are generated at the top contact and in the sample close to the top surface, and are detected at the back contact. The temperature is changed from 80 to 300 K for the 4H-SiC sample and from 220 to 430 K for the diamond sample.

Nd-YAG lasers with 713 Hz repetition frequency and wavelengths of 355 and 213 nm, respectively. This allows a very specific energy selectivity as these wavelengths correspond to a photon energy of 3.49 and 5.82 eV (just above the energy bandgap of the 4H-SiC and diamond, respectively) with absorption lengths of only a few μm.[22] Several interference filters blocked lower harmonics and neutral density filters allowed reducing the intensity to any desired level. As electron–hole pairs are generated only in close proximity to the top contact, it is possible to observe the transport of either holes or electrons (depending on the applied bias polarity) through the sample and extract the charge carriers at the back contact is displayed on the oscilloscope through the amplifier.[23,24] Here, a low-noise broadband current amplifier, with a bandwidth of 1 GHz and a gain of 24 dB, together with a digital storage oscilloscope (DSO) was used. The bias on the top contact was applied using a 50 μs pulser via a bias-tee. The short pulsed bias ensured capacitive voltage distribution across the sample and avoided undesirable sample charging. The samples were mounted on a chip carrier, wire bonded, and placed in a liquid nitrogen cooled Janis ST-100 vacuum cryostat with optical access. A LakeShore 331 temperature controller with a calibrated TG-120-CU-HT-1.4H GaAlAs diode sensor was used in good thermal contact with the sample.

The temperature varied between 80 and 300 K and 220 and 430 K for the 4H-SiC and the diamond sample, respectively. For the 4H-SiC sample, the data were taken every 5 K from 80 to 160 K, and every 10 K from 160 to 300 K. Whereas for the diamond sample, the data were collected every 2 K through the whole temperature range. These temperature ranges were selected during the measurement where a long signal tails were observed. To ensure that the tails of the signal were originated by the de-trapping process, the applied voltages were carefully chosen (120 and 10 V for 4H-SiC and diamond samples, respectively) during the measurement by observing the signal prior to saturation. Also, the voltages were large enough to make a uniform electric field in the samples. The time and the current data, as well as temperature data, were collected during the measurement.

If the sample does not contain impurities, the signal from the measurement should be square-shaped. The time of flight can be calculated by finding the time difference between the start and end points of the signal. Due to charges being trapped and de-trapped, a signal tail can be observed if the sample contains impurities.[21,25] Thus, the defect information can be acquired by investigating the signal tail. By applying the analysis method to the acquired data from the ToF measurement, an Arrhenius plot is given and the defect energy level can be extracted.

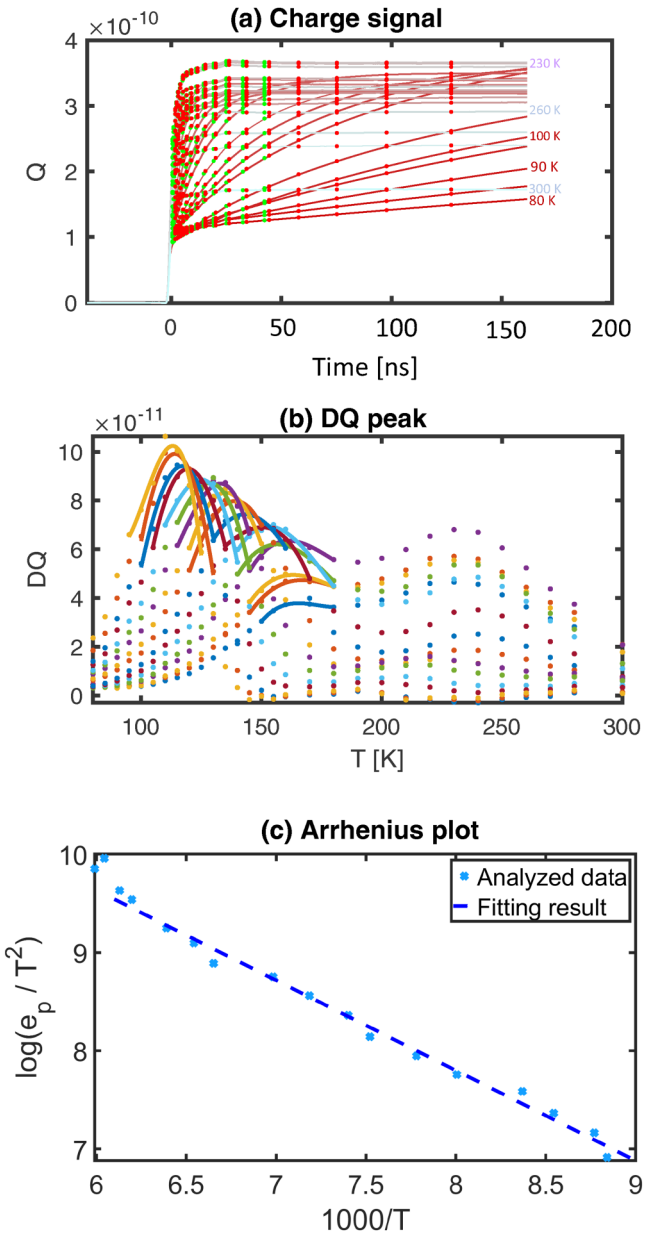

FIG. 2. Illustration of the QTS method. (a) Converting acquired current data to the charge information and making several t_1 and t_2 combinations to find a charge difference on each boxcar. Green dots on the signals are the t_1, and red dots are t_2 for making boxcars. (b) Finding the maximum value of the charge difference and calculate the time constant from the temperature information on each boxcar. (c) Finding the emission rate from the time constant to make an Arrhenius plot to identify the activation energy of the defect.

III. ANALYZING METHODS

A. QTS method

Figure 2 illustrates the QTS method. First, the information from the collected current signal is converted into charge data for each temperature by taking the integral of the current with time,

$$Q = \int_0^t I(t')dt' = \Delta Q_0 \exp(-t/\tau). \tag{1}$$

Here, ΔQ_0 is the charge difference due to the pulse at time $t = 0$, and τ is the time constant. Several sets of time combinations (t_1 and t_2) are prepared, which act as weighting functions so-called "boxcar" [Fig. 2(a)]. The charge difference is then calculated for each boxcar and temperature and can be expressed as

$$DQ(T) = \Delta Q_0\{\exp(-t_1/\tau) - \exp(-t_2/\tau)\}. \tag{2}$$

The DQ peak value is given by plotting the charge difference depending on the temperature [Fig. 2(b)]. Also, from Eq. (2), the time constant of the maximum DQ value is given by differentiating it with respect to τ,

$$\frac{d(DQ)}{d\tau} = \Delta Q_0\left\{\left(\frac{t_1}{\tau}\right)\exp(-t_1/\tau) - \left(\frac{t_2}{\tau}\right)\exp(-t_2/\tau)\right\}, \tag{3}$$

where $\frac{d(DQ)}{d\tau} = 0$, it satisfies $(\frac{t_1}{\tau})\exp(-t_1/\tau) = (\frac{t_2}{\tau})\exp(-t_2/\tau)$. Thus, τ can be calculated as

$$\tau = \frac{ln(t_2/t_1)}{t_2 - t_1} = \frac{1}{e_p}, \tag{4}$$

where e_p is the charge emission rate (here for holes). The emission rate can be expressed by the equation

$$e_p = (\sigma_p \cdot \langle v_p \rangle \cdot N_V) \cdot \exp\left(-\frac{E_a}{kT}\right). \tag{5}$$

Here, σ_p is the capture cross section, $\langle v_p \rangle = (\frac{3kT}{m_h})^{\frac{1}{2}}$ is the mean thermal velocity of holes, $N_V \sim 2(\frac{2\pi m_h kT}{h^2})^{\frac{3}{2}}$ is the effective density of states in the valence band. m_h, k, and E_a are the effective mass of hole, the Boltzmann constant, and the activation energy of the defect respectively. $(\sigma_p \cdot \langle v_p \rangle \cdot N_V)$ in Eq. (5) is proportional to T^2, and therefore, e_p should be divided by T^2 to find a correct activation energy. For simplicity, we assume that the cross section is constant.

Hence, a relation between the emission rate and the defect energy can be driven as below,

$$\frac{e_p}{T^2} \propto \exp\left(-\frac{E_a}{kT}\right). \tag{6}$$

After the emission rates are calculated [Eq. (4)], the activation energies are found by plotting $\ln(e_p/T^2)$ vs $1000/T^2$ [Fig. 2(c)]. This method is widely used to identify defects in semiconductors. However, there are some limitations especially if the sample has multiple defects whose energy levels are very close to each other. It would be difficult to distinguish these complex energy levels because the peaks of the DQ plot might overlap.[26]

B. ILQTS method

Figure 3 shows the illustration of the ILQTS method. This method directly extracts emission rates from the current acquired by the ToF measurement. Thus, no information is lost during the process. This makes it possible to increase the energy resolution when detecting defects in complex systems.[10] Considering the general expression of inverse Laplace transformation;

$$f(t) = \int_0^\infty F(s)\exp(-st)ds. \tag{7}$$

Here, $f(t)$ and $F(s)$ correspond to the current data of the function of time, and the emission rate function, respectively. The current data are fitted by the function below (Also, as seen in Fig. 3),

$$f(t) = \sum_{i=1}^{n} A_i \exp(-e_{pi} \cdot t). \tag{8}$$

In this analysis, inverse Laplace transformation is applied to the fitted function $f(t)$ [Eq. (8)], and $F(s)$ is given as the delta function (the inset in Fig. 3),

$$F(s) = \sum_{i=1}^{n} A_i \delta(s - e_{pi}). \tag{9}$$

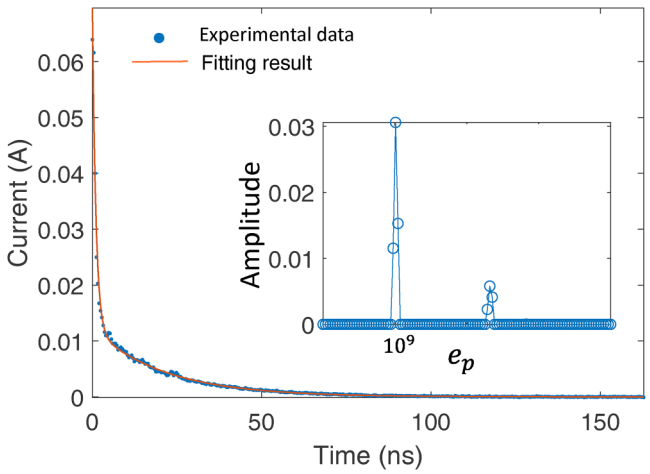

FIG. 3. Illustration of the ILQTS method. The main figure shows the fitting of the current data acquired from the ToF measurement using Eq. (8). The inset shows the applied inverse Laplace transformation [Eq. (9)] to the fitting results.

Finally, the Arrhenius plot is given by extracting the emission rates from Eq. (9).[26] When fitting the current data, the number of exponentials is undetermined. The Tikhonov regularization method[27,28] is used to find the best fit for the current data. This method is used when the target problem does not have a solution or has an infinite number of solutions (ill-posed problem). By minimizing the gap between the solution and the problem, it can find the most probable solution for fitting the current data.

IV. RESULTS AND DISCUSSION

A. Sample characterizations

Raman spectroscopy using a 532 nm YAG laser was performed at room temperature on both samples to check the crystal quality conditions. The samples were exposed by the laser, 30 s and 10 s for the 4H-SiC and the diamond sample, respectively. Figures 4(a) and 4(b) show the result of Raman spectroscopy of the 4H-SiC and diamond sample, whereas the insets show the cross-polar images of each material, respectively. The strong signal intensity of the Raman spectrum in diamond indicates high crystal quality and the absence of impurities with significant concentration.[29] Folded transversal acoustic (E_2 (TA)), folded longitudinal acoustic (A_1 (LA)), folded transversal optical (E_2 (TO)), and longitudinal optical phonon (A_1 (LO)) peaks were observed in the 4H-SiC sample. The observation gives valuable information about the phonon band structure of the SiC crystal and the polytype, which is, in this case, 4H. In addition, the Raman spectrum reveals that the surface of the 4H-SiC sample is parallel to the c -axis and the crystal is undoped.[30] Observation from the cross-polar shows some structural defects in the samples, especially in the diamond sample. Some four-petalled patterns in the cross-polar were observed in the diamond sample. These defects are due to the dislocations.[31] Also, a couple of bright shadows were observed in the middle/upper left of the figure. These are due to the presence of strain in the diamond crystal evolved during the growth process. From the image, it can be concluded that there are no critical structural defects on the sample that affect the measurement. For the 4H-SiC sample, due to its hexagonal crystal structure, it was difficult to analyze the structure defects. In both cases, the mesh contacts were placed in the middle of the samples to avoid the most critical part.

In addition to Raman spectroscopy, x-ray photoelectron spectroscopy (XPS) and time-of-flight energy elastic recoil detection analysis (ToF-E ERDA) were performed, and the results are shown in Figs. 4(c), 4(d), 4(e), and 4(f).

For XPS, a beam size of 200 μm in diameter and a power of 50 W were used. The survey spectrum of XPS on the 4H-SiC sample showed not only the silicon (Si2p) and carbon (C1s) spectra, but also showed oxygen (O1s and O KLL) spectra. Depth profiling was also performed by using an Ar^+ ion gun with an energy of 1 kV every minute before taking intensity data of the target molecules. This process was repeated at ten intervals. As a result, the oxygen was found to be concentrated on the very surface of the sample. The same configuration was used for the XPS on the diamond sample. Five intervals were employed instead of ten when making depth profiling. Argon spectra (Ar2s and Ar2p3) and a nitrogen spectrum (N1s) were found, as well as carbon spectra (C1s) on the result. Argon spectra started to appear after the Ar

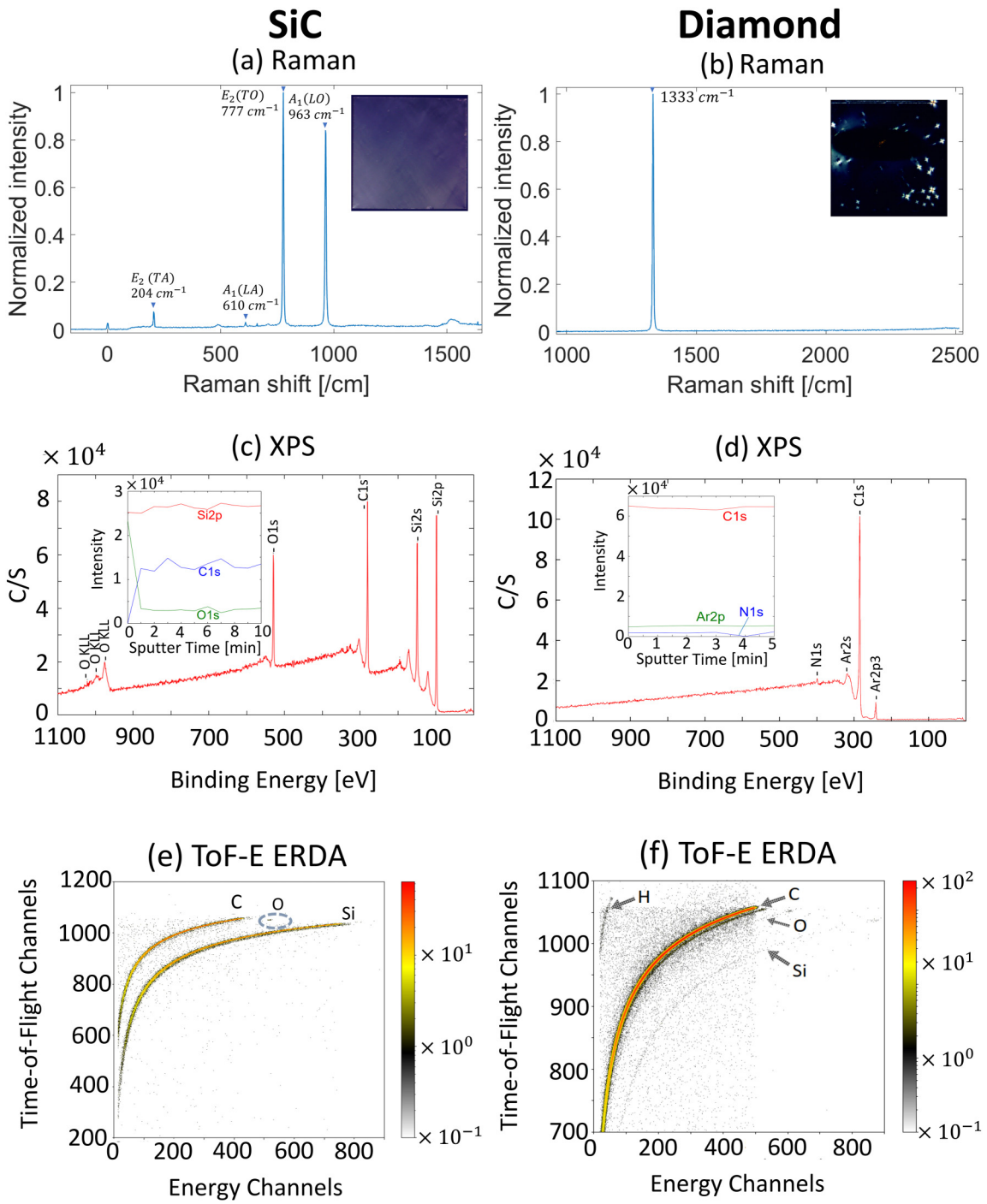

FIG. 4. The results of [(a) and (b)] Raman, [(c) and (d)] XPS, and [(e) and (f)] ToF-E ERDA for the 4H-SiC (left) and the diamond (right) sample. The Raman spectra [(a) and (b)] show the 4H-SiC polytype and a sharp diamond peak. From the Raman spectra, no intentional doping was found. The insets show the cross-polar image of the samples. XPS spectra show the presence of oxygen (O1s and O KLL) in the 4H-SiC sample. The oxygen was found to be concentrated close to the surface of the sample. In the diamond sample, traces of argon (Ar2s and Ar2p3) and nitrogen (N1s) were seen in the XPS result. The insets in the XPS figure show the depth profiling. For ToF-E ERDA, the oxygen impurity was found to be present only close to the surface of the 4H-SiC sample as well as the XPS result. Oxygen, hydrogen, and silicon impurities were found in the diamond sample.

sputtering. We assume that this is because the Ar atoms were migrated into the diamond lattice by sputtering.[32]

ToF-E ERDA was conducted using 36 MeV I as a probing beam.[33] The detector was placed 45° with respect to the incoming beam. More information on the experimental procedure can be found in Moldarev *et al.*[34] The result of the 4H-SiC sample shown in Fig. 4(e) confirmed that oxygen was found only on the surface of the sample. The averaged composition rate for the 4H-SiC in the region of interest (500–2500 [10^{15} atoms/cm^2]) was 51.1 ± 0.3% for silicon and 48.9 ± 0.3% for carbon, respectively. The same configuration was used for the diamond sample, and oxygen, hydrogen and silicon impurities were found as impurities. In the case of the diamond sample, the composition rate (500–2000 [10^{15} atoms/cm^2]) was measured to be 0.08 p/m 0.01% for hydrogen, 99.7 ± 0.4% for carbon, 0.16 ± 0.02% for oxygen, and 0.04 p/m 0.01% for silicon. Even though the results of the diamond sample in XPS and ToF-E ERDA show different impurities, those impurities are expected. The CVD growth of diamonds requires an environment of a hydrogen-rich atmosphere. Hydrogen is included to lower the surface energy and stabilize the growing crystal. A small amount of oxygen is also often added during the growth to enhance the crystalline quality. Therefore, hydrogen and oxygen impurities are normally present in the CVD diamond.[35]

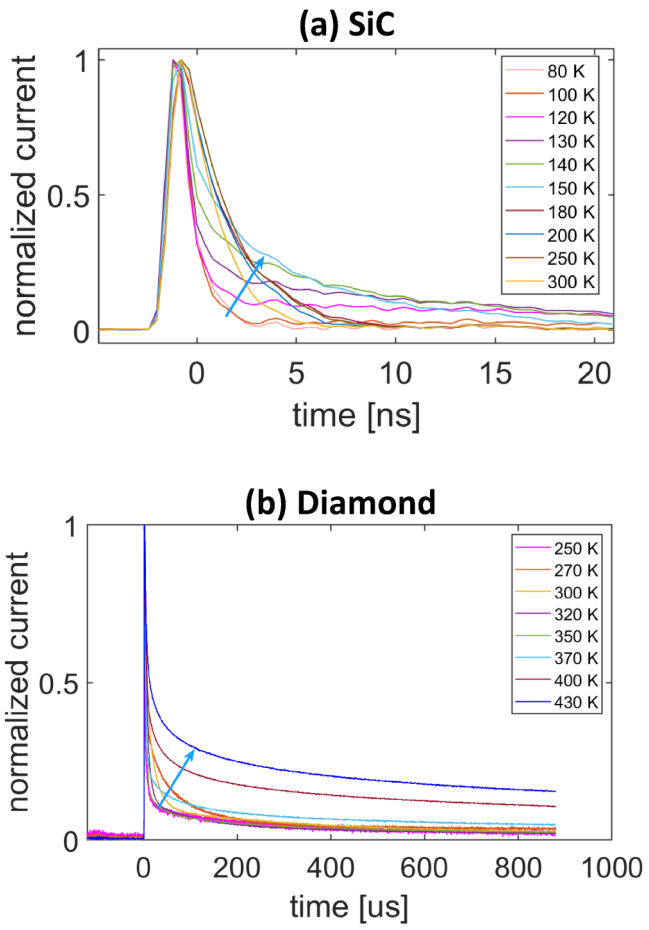

FIG. 5. Current data acquired by the ToF measurement on (a) the 4H-SiC sample at 120 V and (b) the diamond sample at 10 V. The longer tail was found from 120 to 150 K from ToF measurement on the 4H-SiC sample, and in the entire temperature range on the diamond sample. These tails were caused by the delayed charges trapped and subsequently de-trapped by defects. Blue arrows indicates the tendency of the tails to shift with temperature.

B. ToF results

Figure 5 shows the current acquired by the ToF measurement with a voltage of 120 V applied across the 4H-SiC and 10 V across the diamond. To show the comparison of signal tails at different temperatures, the normalized current is shown in the figure. Also, only the current data at the specific temperatures whose signal tails are obvious were selected in the figure. For 4H-SiC, the signal looks similar for all temperatures, and a peak was observed in the beginning and a tail follows the peak. The tails at temperatures from 120 to 150 K were observed to be longer than those at other

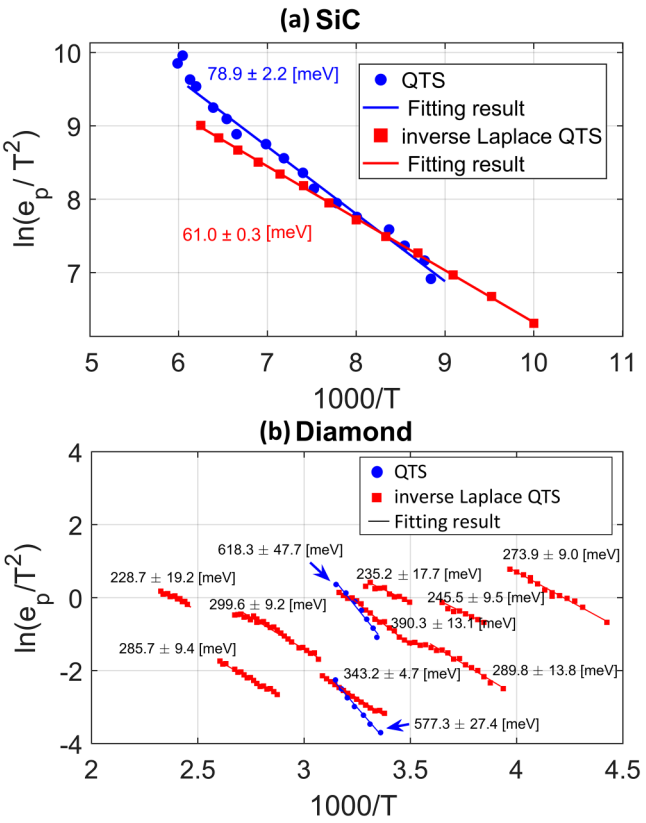

FIG. 6. Arrhenius plot of (a) the 4H-SiC and (b) the diamond sample that were analyzed by the QTS and ILQTS methods. In the Arrhenius plots, the blue circles show the result of the QTS method. The red square marker shows the result of the ILQTS method. Fitting results are shown in straight lines. Energy levels above the valence band are written adjacent to each fitting result.

temperatures. On the other hand, for diamond, long tails were observed in the micro-second range in the entire temperature from 220 to 430 K. Tails observed in the measurement were caused by the carriers trapped by the defects being de-trapped. Here, the decay tails in the signal tails are considered to originate only in the carrier emission. As soon as there are mobile carriers, they instantaneously contribute to the measured current (except for the negligible time delay that is due to the finite speed of light). This is because mobile carriers in a dielectric induce a current on the receiving electrode. This is described by the Shockley–Ramo theorem and is explained in, e.g., W. Shockley[36] and Ramo.[37] The bias voltages have been chosen high enough to provide a high charge collection efficiency, but low enough to make the field emission from traps negligible. Also, the voltages were large enough to make a uniform electric field in the samples. However, the electric field distribution is not critical as long as the charge collection efficiency is high.

C. Analysis by QTS and ILQTS methods

Figure 6 shows the Arrhenius plots given by the QTS and the ILQTS analysis for (a) the 4H-SiC and (b) the diamond sample. Here, all temperature points were considered in the analysis. The slopes of the Arrhenius plot for the 4H-SiC sample were observed roughly from 100 to 150 K, which corresponds to the temperature range where the long tails were found in the ToF result. The defect energy level found was at $E_V + (78.9 \pm 2.2)$ meV and $E_V + (61.0 \pm 0.3)$ meV using QTS and ILQTS methods, respectively. The energy levels related to the presence of oxygen in 4H-SiC were previously calculated by Matsushita *et al.*[38] and show energy levels similar to our result. The optical measurement also supports the result. Thus, the impurity in the 4H-SiC sample can be concluded to be oxygen. There is, however, an energy level difference detected between the two methods. In the QTS method, the fitting was done on the charge difference (DQ) when finding the time constant from its maximum value. Here, the fitting quality depends on how many temperature points are taken in the measurement and also on the fitting formula itself. The quality of the linear fitting on the Arrhenius plot depends on the number of points on the plot, which is decided by the number of boxcars. Optimization of those parameters might have affected the final result.

For the diamond sample, we identified more slopes using the ILQTS compared to QTS. Two slopes from the QTS method could be seen in the temperature interval at 300–320 K. The fitting results were $E_V + (618.3 \pm 47.7)$ meV and $E_V + (577.3 \pm 27.4)$ meV. Nine different energy states from the minimum $E_V + (228.7 \pm 19.2)$ meV to the maximum $E_V + (390.3 \pm 13.1)$ meV were extracted from the ILQTS method in the entire temperature range. The reason why the ILQTS method showed more energy levels is due to the presence of multiple peaks in the vicinity of each other. As several peaks were very close to each other in the DQ plot, they could not be distinguished, which caused an averaging of energy states. Although it was difficult to identify each energy level from the optical measurements and the existing references, the result shows that the ILQTS method has some advantages compared to the QTS method. More precise analysis requires considering the temperature dependence of the capture cross section. This will surely provide more detailed information to address the specific defect. In addition, the entropy term is important to consider the analysis more carefully.[39] The relation among the Gibbs free energy (G), entropy (S), and enthalpy (H) is expressed as $\Delta G = \Delta H - T\Delta S$, where T is the temperature. By containing those terms in the analysis, Eq. (5) becomes $e_p = (\sigma_p \cdot \langle \nu_p \rangle \cdot N_V) \cdot \exp(-\frac{\Delta H - T\Delta S}{kT})$. This means that the entropy term ΔS should appear in the y intercept as $\ln(\sigma_p \cdot \langle \nu_p \rangle \cdot N_V) + \frac{\Delta S}{k}$. The equation depends both on entropy and the cross section. Additional measurements are required to determine them separately.

The ILQTS method was proven to be more sensitive with a higher resolution than the QTS method, however, it has some downsides depending on the conditions. One of the conditions required for the successful usage of the ILQTS method is to have enough temperature points. As this method directly extracts information from the current data at each temperature, it would not detect defects if there are not enough temperature points taken from the measurement in the region of interest. Furthermore, the method requires more computational power for the analysis to find the best fit for the current data. The more temperature points exist, the longer time is required to perform the data analysis.

V. CONCLUSIONS

Charge transient spectroscopy techniques using 3.49 and 5.82 eV laser illumination were applied to investigate undoped 4H-SiC and diamond. The QTS and ILQTS analysis methods were performed on the measurement data. We observed an energy level from the QTS and ILQTS method that correspond to the oxygen defects in 4H-SiC. Electrically active impurities in high-resistive and undoped materials are difficult to investigate using the conventional DLTS method. Based on the results, we can conclude that the charge transient spectroscopy (ToF) technique, using optically induced charge excitation, is a good candidate as an alternative technique to DLTS. Also, both methods were found to be applicable for analyzing the result of this technique. For diamond, two energy levels were found from the QTS method, whereas nine different energy states were detected by the ILQTS method. Although the nature and originality of these energy states are not yet addressed, the sensitivity of the ILQTS method can be seen to be higher than that of QTS. The observed energy states, however, require further in-depth investigation.

ACKNOWLEDGMENTS

The Swedish Energy Agency (Grant No. 1) and the Swedish Research Council (Grant No. 04186-5) are gratefully acknowledged for financial support. In addition, Carl Tryggers Foundation (CTS 24:3542) are gratefully acknowledged by the authors.

AUTHOR DECLARATIONS

Conflict of Interest

The authors have no conflicts to disclose.

Author Contributions

Rina Yamazaki: Formal analysis (equal); Investigation (equal); Validation (equal); Writing – original draft (equal); Writing – review & editing (equal). **Jan Isberg:** Conceptualization (equal); Investigation (equal); Supervision (equal); Validation (equal); Writing – review & editing (equal). **Nattakarn Suntornwipat:** Supervision (equal); Validation (equal); Writing – review & editing (equal). **Dmitrii Moldarev:** Formal analysis (equal); Investigation (equal); Writing – review & editing (equal). **Björn Magnusson:** Formal analysis (equal); Resources (equal); Writing – review & editing (equal). **Aisuluu Aitkulova:** Writing – review & editing (equal). **Saman Majdi:** Conceptualization (equal); Funding acquisition (equal); Methodology (equal); Supervision (equal); Writing – review & editing (equal).

DATA AVAILABILITY

The data that support the findings of this study are available from the corresponding author upon reasonable request.

REFERENCES

[1]B. Setera and A. Christou, "Challenges of overcoming defects in wide bandgap semiconductor power electronics," Electronics **11**, 10 (2022).
[2]D. V. Lang, "Deep-level transient spectroscopy: A new method to characterize traps in semiconductors," J. Appl. Phys. **45**, 3023–3032 (1974).
[3]P. Blood and J. W. Orton, "The electrical characterisation of semiconductors," Rep. Prog. Phys. **41**, 157 (1978).
[4]E. Simoen, P. Clauws, and J. Vennik, "The determination of deep level concentrations in high resistivity semiconductors by DLTS, with special reference to germanium," J. Phys. D: Appl. Phys. **18**, 2041 (1985).
[5]J. Laird, R. Bardos, C. Jagadish, D. Jamieson, and G. Legge, "Scanning ion deep level transient spectroscopy," Nucl. Instrum. Methods Phys. Res. Sec. B **158**, 464–469 (1999).
[6]W. Kada, Y. Kambayashi, Y. Ando, S. Onoda, H. Umezawa, Y. Mokuno, S. Shikata, T. Makino, M. Koka, O. Hanaizumi, T. Kamiya, and T. Ohshima, "Investigation of electrically-active deep levels in single-crystalline diamond by particle-induced charge transient spectroscopy," Nucl. Instrum. Meth. Phys. Res. Section B **372**, 151–155 (2016).
[7]C. Ye and J. H. Chen, "Studies of defects in n-type CdTe by charge transient spectroscopy," J. Appl. Phys. **67**, 2475–2481 (1990).
[8]N. Iwamoto, A. Koizumi, S. Onoda, T. Makino, T. Ohshima, K. Kojima, S. Koike, K. Uchida, and S. Nozaki, "Defects in an electron-irradiated 6H-SiC diode studied by alpha particle induced charge transient spectroscopy: Their impact on the degraded charge collection efficiency," Mater. Sci. Forum **717–720**, 267–270 (2012).
[9]W. Kada, Y. Kambayashi, N. Iwamoto, S. Onoda, T. Makino, M. Koka, T. Kamiya, N. Hoshino, H. Tsuchida, K. Kojima, O. Hanaizumi, and T. Ohshima, "Development of diagnostic method for deep levels in semiconductors using charge induced by heavy ion microbeams," Proc. 14th Inter. Conf. Nucl. Micro. Technol. Appl. 2014 **348**, 240–245 (2015).
[10]L. Dobaczewski, A. R. Peaker, and K. Bonde Nielsen, "Laplace-transform deep-level spectroscopy: The technique and its applications to the study of point defects in semiconductors," J. Appl. Phys. **96**, 4689–4728 (2004).
[11]L. Dobaczewski, P. Kaczor, I. D. Hawkins, and A. R. Peaker, "Laplace transform deep-level transient spectroscopic studies of defects in semiconductors," J. Appl. Phys. **76**, 194–198 (1994).
[12]S. Koike, K. Uchida, and S. Nozaki, "Deep level characterization improved by laplace charge transient spectroscopy," Inter. J. Eng. Appl. Sci. **5**, 66–69 (2018).
[13]Ł. Gelczuk, M. Dąbrowska-Szata, V. Kolkovsky, M. Sochacki, J. Szmidt, and T. Gotszalk, "Origin and anomalous behavior of dominant defects in 4h-siC studied by conventional and laplace deep level transient spectroscopy," J. Appl. Phys. **127**, 064503 (2020).
[14]A. A. Lebedev, "Deep level centers in silicon carbide: A review," Semiconductors **33**, 107–130 (1999).
[15]T. Dalibor, G. Pensl, H. Matsunami, T. Kimoto, W. J. Choyke, A. Schöner, and N. Nordell, "Deep defect centers in silicon carbide monitored with deep level transient spectroscopy," Phys. Status Solidi (a) **162**, 199–225 (1997).
[16]K. K. Kovi, S. Majdi, M. Gabrysch, and J. Isberg, "A charge transport study in diamond, surface passivated by high-k dielectric oxides," Appl. Phys. Lett. **105**, 202102 (2014).
[17]J. Isberg, S. Majdi, M. Gabrysch, I. Friel, and R. S. Balmer, "A lateral time-of-flight system for charge transport studies," Diamond Relat. Mater. **18**, 1163–1166 (2009).
[18]J. Isberg, M. Gabrysch, J. Hammersberg, S. Majdi, K. K. Kovi, and D. J. Twitchen, "Generation, transport and detection of valley-polarized electrons in diamond," Nat. Mater. **12**, 760–764 (2013).
[19]S. Majdi, M. Gabrysch, K. K. Kovi, N. Suntornwipat, I. Friel, and J. Isberg, "Low temperature conduction-band transport in diamond," Appl. Phys. Lett. **109**, 162106 (2016).
[20]M. Gabrysch, S. Majdi, D. J. Twitchen, and J. Isberg, "Electron and hole drift velocity in chemical vapor deposition diamond," J. Appl. Phys. **109**, 063719 (2011).
[21]M. Funahashi, "Time-of-flight method for determining the drift mobility in organic semiconductors," in *Organic Semiconductors for Optoelectronics* (Wiley Semiconductors, 2021), pp. 161–178.
[22]V. Djurberg, S. Majdi, N. Suntornwipat, and J. Isberg, "Investigation of photo-excitation energy impact on electron mobility in single crystalline CdTe," Materials **14**, 4202 (2021).
[23]N. Suntornwipat, M. Gabrysch, S. Majdi, D. J. Twitchen, and J. Isberg, "Magnetotransport study of valley-polarized electrons in synthetic diamond," Phys. Rev. B **94**, 035408 (2016).
[24]N. Tranchant, M. Nesladek, D. Tromson, Z. Remes, A. Bogdan, and P. Bergonzo, "Time of flight study of high performance CVD diamond detector devices," Phys. Status Solidi (a) **204**, 3023–3029 (2007).
[25]M. Martini, J. W. Mayer, and K. R. Zanio, *Drift Velocity and Trapping in Semiconductors-Transient Charge Technique* (Elsevier, 1972), pp. 181–261.
[26]M. N. Levin, A. E. Bormontov, A.. Akhkubekov, and E. A. Tatokhin, "Relaxation spectroscopy of deep levels in semiconductors: Laplace-DLTS method," Tech. Phys. Lett. **36**, 1001–1005 (2010).
[27]J. Weese, "A reliable and fast method for the solution of Fredhol integral equations of the first kind based on Tikhonov regularization," Comput. Phys. Commun. **69**, 99–111 (1992).
[28]J. Honerkamp and J. Weese, "Tikhonovs regularization method for ill-posed problems," Continuum. Mech. Thermodyn. **2**, 17–30 (1990).
[29]A. Zaitsev, *Optical Properties of Diamond: A Data Handbook*. 1st ed. (Springer, Berlin, 2001).
[30]M. Bauer, A. M. Gigler, A. J. Huber, R. Hillenbrand, and R. W. Stark, "Temperature-depending Raman line-shift of silicon carbide," J. Raman Spectros. **40**, 1867–1874 (2009).
[31]H. Pinto and R. Jones, "Theory of the birefringence due to dislocations in single crystal CVD diamond," J. Phys.: Condens. Matter **21**, 364220 (2009).
[32]J.-F. Veyan, E. d. Obaldia, J. J. Alcantar-Peña, J. Montes-Gutierrez, M. J. Arellano-Jimenez, M. J. Yacaman, and O. Auciello, "Argon atoms insertion in diamond: New insights in the identification of carbon C 1s peak in x-ray photoelectron spectroscopy analysis," Carbon **134**, 29–36 (2018).
[33]P. Ström and D. Primetzhofer, "Ion beam tools for nondestructive *in-situ* and *in-operando* composition analysis and modification of materials at the Tandem Laboratory in Uppsala," J. Instrum. **17**, P04011 (2022).
[34]D. Moldarev, D. Primetzhofer, C. C. You, S. Z. Karazhanov, J. Montero, F. Martinsen, T. Mongstad, E. S. Marstein, and M. Wolff, "Composition of photochromic oxygen-containing yttrium hydride films," Solar Energy Mater. Solar Cells **177**, 66–69 (2018).

[35]S. J. Sque, R. Jones, and P. R. Briddon, "Structure, electronics, and interaction of hydrogen and oxygen on diamond surfaces," Phys. Rev. B **73**, 085313 (2006).
[36]W. Shockley, "Currents to conductors induced by a moving point charge," J. Appl. Phys. **9**, 635–636 (1938).
[37]S. Ramo, "Currents induced by electron motion," Proc. IRE **27**, 584–585 (1939).
[38]Y. Matsushita, Y. Furukawa, Y. Hijikata, and T. Ohshima, "First-principles study of oxygen-related defects on 4H-SiC surface: The effects of surface amorphous structure," Appl. Surf. Sci. **464**, 451–454 (2019).
[39]H. Brooks, *Theory of the Electrical Properties of Germanium and Silicon* (Academic Press, 1955), pp. 85–182.